agriculture

MDPI

*Article*

# Design and Parameter Optimization of Rotary Double-Insertion Device for Small Arched Insertion Machine

**Jianling Hu, Yan Gong * and Xiao Chen**

Nanjing Institute of Agricultural Mechanization, Ministry of Agriculture and Rural Affairs, Nanjing 210014, China; 82101215525@caas.cn (J.H.); chenxiao@caas.cn (X.C.)
* Correspondence: gongyan@caas.cn

**Abstract:** China's small arched shed-building machinery suffers from a low degree of mechanization, building efficiency, and qualification rate for frame insertion. Therefore, we designed a rotary double-insertion device and established the equation for its motion trajectory. The analysis shows that in the rotary insertion process, a better point of entry into the soil exists. A simulation model was constructed in ADAMS, and the static and dynamic trajectories were analyzed. Additionally, the optimal planting and insertion speed ratios were determined. Considering the qualified rate of the insertion frame as the evaluation index to establish a regression model, we adopted a three-factor three-level experimental design and established the planting speed ratio, center distance of the planting arm, and length of the pressing rod arm as the main influencing factors. We used Design-Expert 13 to perform the analysis of variance and determined the optimal parameter combinations. The experimental results show that the planting speed ratio was 0.7, the center distance of the planting arm group was 554 mm, the length of the pressing rod arm was 923 mm, and the qualification rate of trellis planting at this time was 98.05%. The bench was adjusted and tested based on the optimal parameter combination. The average value of the measured trellis qualification rate was 96.73%, and the relative error between the test value and the theoretical optimization value was 1.32%, thereby verifying the reliability of the optimal parameter combination. Field verification test results show that the rotary double-insertion device had a planting speed ratio of 0.7 and a trellis qualified rate of 95.74% compared with the theoretical optimization value of 2.31%. Conforming to the design requirements of small arch shed-building machinery, the prototype operation performance was stable.

**Keywords:** experimental design; parameter optimization; rotary double-insertion device; small arched shed; small arched shed-building machinery



**Citation:** Hu, J.; Gong, Y.; Chen, X. Design and Parameter Optimization of Rotary Double-Insertion Device for Small Arched Insertion Machine. *Agriculture* **2024**, *14*, 739. https://doi.org/10.3390/agriculture14050739

Academic Editor: Caiyun Lu

Received: 19 April 2024
Revised: 6 May 2024
Accepted: 7 May 2024
Published: 9 May 2024



## 1. Introduction

Currently, the area of facility horticulture in China is 3.7 million hm$^2$, of which the area of arched greenhouses (including large, medium, and small arched sheds) is 2.7 million hm$^2$ [1]. Among the types of arched greenhouses, small arched sheds, characterized by low cost and good adaptability, are widely used for the cultivation of vegetables, melons, fruits, and other horticultural crops [2,3]. For example, small arched greenhouses are usually used for growing strawberries [4]. Compared with open field cultivation, chaparral induces high humidity and high air and soil temperatures in the shed [5–8], thereby promoting strong crop emergence [9,10]. Meanwhile, it protects crops in the early developmental stages [11,12]; reduces leaf infestation by weeds, pathogens, and pests [13,14]; and improves yield and quality [15]. In addition, small arches can allow crops to advance or delay the growth cycle [16]. This extends the harvesting period [17,18] and allows fruits and vegetables to defy the growth rules of the natural seasons and satisfy the market demands throughout the year, thus affording higher economic benefits from cultivation [19–21]. For example, in winter, small arches can prevent frost [22]. By combining scaffolding and plastic film, the temperature inside the arches can be increased by 1–4 °C more than the

external temperature during frost; thus, small arched greenhouse cultivation technology can better reduce the frost risk [23]. The low profile of the small arches allows farmers to begin planting and harvesting earlier and to sell their crops at higher prices before the prices start to fall mid-season [24].

Small arched trellis construction primarily depends on manual labor such as selecting flexible bamboo or wood strips as the skeleton of the arched trellis materials, bending both ends and inserting them into the soil to form an arch, covering it with plastic film for thermal insulation and moisture preservation to prevent wind and freezing disasters, and building a simple small arched trellis [25]. The traditional manual approach to building small arched greenhouses entails the use of skeleton materials from various sources and incurs relatively low cost. However, before building, trellis poles should be precisely sized and manually bent and planted, ensuring consistent spacing of the arches of the skeleton of the arched greenhouse. This implies high labor intensity but low operational efficiency [26]. The arch-shaped trellis poles thus planted may not be uniformly covered by the film, and the tension to reduce the overall wind resistance of the small arched greenhouses may be insufficient. The overall wind resistance and firmness of the small arched shed are therefore difficult to ensure. Natural materials such as bamboo chips or wood strips are difficult to use in machinery. In contrast, fiberglass poles are industrial products with uniform dimensions and good compressive and bending resistances; therefore, these are selected as the alternative to bamboo chips for the trellis pole material.

Currently, there are a few frame-insertion machines in operation in China. The degree of intelligence is high; however, as regards the use of the downward-pressing frame-insertion mechanism after stopping and planting, the operation speed is low. Simultaneously, because of the complexity of the mechanical structure and control system, the manufacturing cost is considerably high [27]. Large-scale small arched greenhouse building machinery with rotary insertion mechanisms, exhibiting improved insertion efficiency, are commercially available in international markets. However, their design is overly complex. Moreover, they support the use of metal poles and are primarily adapted to large-area field operations and manufacturing; furthermore, they are expensive [28]. Therefore, the design of a simple structure that has a high operating efficiency and that supports fiberglass poles is crucial. Such structures can be used together with the rotary double-insertion device to promote the application of small arched shed cultivation technology.

We constructed the simulation model of a rotary double-insertion device by analyzing the motion trajectory of the rotary insertion device. Further, we analyzed its static and dynamic operation trajectories, and the optimal planting and insertion speed ratios were determined. We established a regression model with the qualified rate of insertion as the evaluation index and adopted a three-factor three-level experimental design to determine the optimal parameter combinations. The structure and working parameters were optimized to verify the operational performance, thus obtaining a reference for the design of efficient machinery for building small arched greenhouses.

## 2. Materials and Methods

### *2.1. Rotary Double-Insertion Device Structure and Working Principle*

Long and straight fiberglass poles (Length 1600 mm, diameter 6 mm, manufactured by Dongguan Fengyuan New Material Technology Co., Ltd., headquartered in Dongguan, China), were bent into arches and then inserted into the soil as a skeleton for building small arches. Such bent poles are hereinafter referred to as trellises. The structural principle of the hanging small arched trellis insertion machine is illustrated in Figure 1. The machine mainly comprises a traveling device, a rotary double-insertion device, trenching shovel, sensor (XL-1808-N, manufactured by Shenzhen Jinhong Electric Appliance Co., Ltd., headquartered in Shenzhen, China), and a trellis pole automatic feeding device. Long and straight trellis poles are placed in the trellis pole automatic feeding device storage hopper; the trellis pole automatic feeding device pre-pitches a straight pole; the tractor suspension body drives forward; the wheels pass through the chassis walking device in the sprocket chain drive

mechanism; the power is transmitted to the insertion of the frame mechanism; the rotary double-insertion of the frame device movement grasps the pre-pitching of the trellis pole bending and inserts it into the soil, according to the rotary process and the sensor judgment. During the rotary process, the sensor determines the position of the rotary double-insertion device, and the control system receives the signal and controls the automatic feeder device to continue to place the poles, waiting for the rotary double-insertion device to grab the poles for bending and insertion.

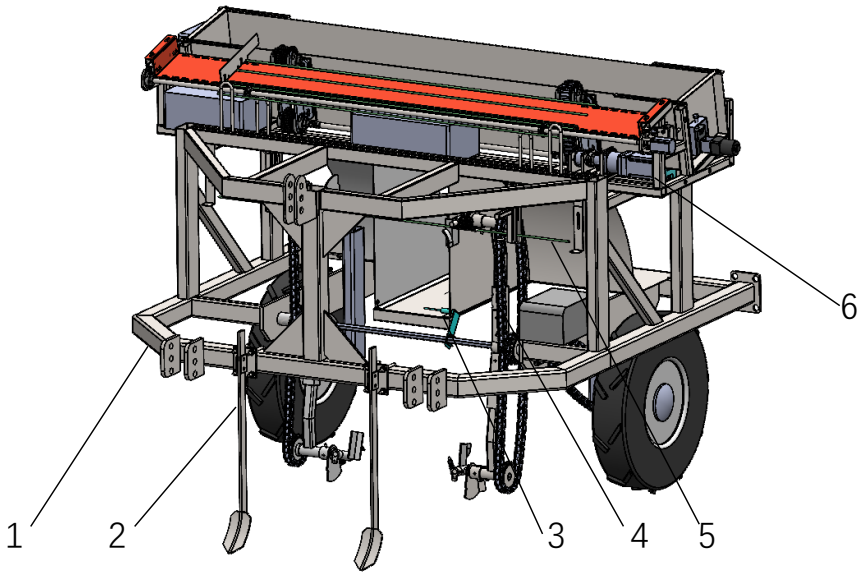


**Figure 1.** Structure of hanging vault continuous arched shed machine. (1) Walking device; (2) trenching shovel; (3) sensor; (4) rotary double-insertion device; (5) trellis pole; and (6) automatic feeder for shed poles.

In accordance with the physical properties of the trellis pole material and building requirements of the small arched shed, we designed a rotary double-insertion device, as shown in Figure 2. It mainly comprises two groups of planting arms, the center rotating shaft, planetary sprocket, the rear drive sprocket, and the inductor plate. The two groups of planting arms are fixed to the center rotating shaft by using bolts, and they operate cooperatively to complete the bending and planting action of the straight greenhouse pole. The design of two groups of planting arms is conducive to maintaining the smooth operation of the mechanism while effectively utilizing the space of the equipment, reducing the rotary waiting time, and improving the efficiency of planting.

The key mechanism of the planting arm in the rotary double-insertion device, as shown in Figure 3, involves a bending bracket, compression rod arm shaft, reset spring, bending pressure plate, and bending bearing plate. The pressing rod arm shaft 3 is hinged to the bending bracket (1), the bending press plate (6) is bolted to the bending bracket (1), the runner (8) and pull ring (5) are mounted on the pressing rod arm (7), the reset spring (4) connects the bending bearing plate (2) and pull ring (5), and the limit lever (9) is welded to the pressing rod arm shaft (3). When the center shaft rotates, the planetary sprocket is driven by the chain to rotate. This, in turn, transmits the power to the pressing rod arm shaft (3), driving it to rotate. Meanwhile, the runner (8) is squeezed by the bending plate (6), bending the shed rod to form an arch.

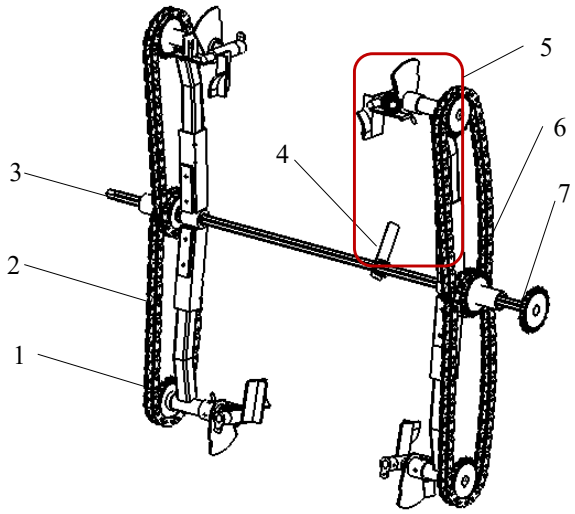


**Figure 2.** Schematic of the structure of the rotary double-insertion device. (1) Planetary sprockets; (2) sprockets; (3) axis of rotation; (4) inductor plate; (5) planting arm; (6) sun sprocket; and (7) rear drive sprocket.

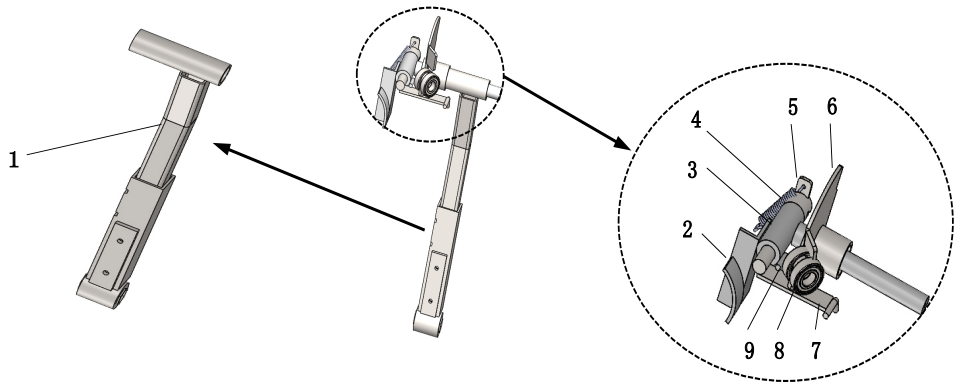


**Figure 3.** Planting arm model diagram. (1) Bending bracket; (2) bending bearing plate; (3) pressing rod arm shaft; (4) reset spring; (5) pull ring; (6) bending plate; (7) pressing rod arm; (8) runner; and (9) limit lever.

### *2.2. Kinematic Analysis of Rotary Double-Insertion Device*

The traveling motion of the machine and rotations of the parts are combined into a compound motion [29]. As the planting arm performs the field operation, the motion of the bending bracket precisely conforms to the compound motion. The traveling direction of the machine is considered the negative *X*-axis direction, while the upward direction perpendicular to the *X*-axis, over the center of the rotary axis, is considered the positive *Y*-axis direction. Accordingly, the trajectory of the end of the bending bracket during operation is depicted in Figure 4.

The trajectory equation of any point on the bending bracket can be expressed as

$$\begin{cases} x = v_m t + R\cos\omega t \\ y = H - R\sin\omega t \end{cases}, \quad (1)$$

where $t$ is the planting arm rotation time (s). Further, $v_m$ denotes the machine travel speed (m/s); $\omega$ is the angular speed of rotation of the bending bracket (rad/s); $R$ denotes the radius of rotation of the bending bracket (m); $\lambda$ is the ratio of the rotational linear velocity of the bending bracket to the forward speed of the machine; and $H$ is the vertical distance from the center of the spindle to the end of the bending bracket (m).

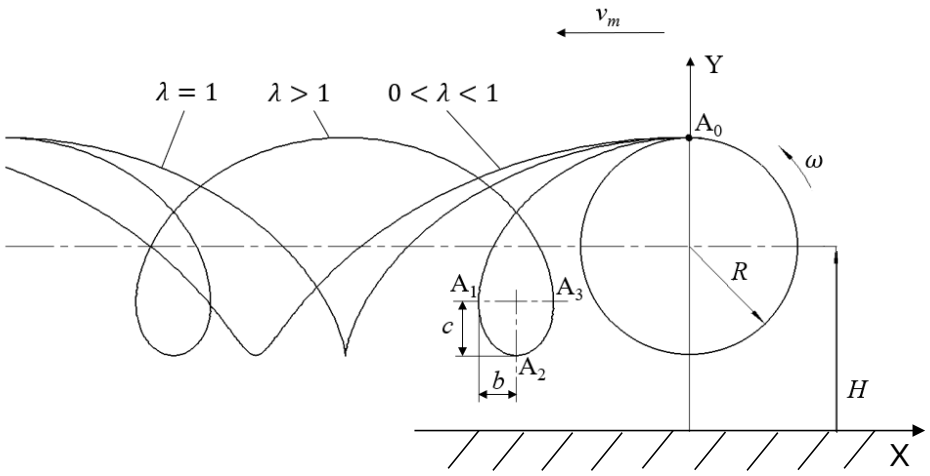


**Figure 4.** Bending bracket trajectory. Note: $v_m$ is the machine travel speed (m/s); $\omega$ represents the angular speed of rotation of the bending bracket (rad/s); $R$ represents the radius of rotation of the bending bracket (m); $\lambda$ denotes the ratio of the rotational linear velocity of the bending bracket to the forward speed of the machine; and $H$ is the vertical distance from the center of the spindle to the end of the bending bracket (m).

The horizontal and vertical partial velocities of the bending bracket at the point are obtained by derivation according to Equation (1) as

$$\begin{cases} v_x = \frac{dx}{dt} = v_m - R\omega \sin \omega t \\ v_y = \frac{dy}{dt} = -\omega R \cos \omega t \end{cases}. \quad (2)$$

The characteristic parameter $\lambda$ is defined as follows:

$$\lambda = \frac{\omega R}{v_m}. \quad (3)$$

The value of $\lambda$ determines the motion trajectory of any point on the bending bracket [30], as shown in Figure 4. For $0 < \lambda < 1$, the motion trajectory of the bending stent is an upper-open parabola without a buckle. For $\lambda = 1$, the bending stent trajectory corresponds to that of an ordinary pendulum between the critical range of the buckle. Further, for $\lambda > 1$, the motion trajectory of the bending stent is a residual pendulum with a buckle. The tangential direction of any point on the curve of the trajectory at any instant denotes the direction of the velocity of the bending bracket at that point. During the process of planting and inserting the poles, the bending bracket must insert the poles into the soil and push them backward in order to utilize the film-laying tension in the mulching stage to return the poles to the upright position. At this stage, the bending support should have a horizontal partial velocity opposing the forward direction of the machine. As shown in Figure 4, for $0 < \lambda \leq 1$, all points on the trajectory of the bending bracket do not have a backward horizontal partial velocity; this does not satisfy the requirements of the insertion operation and is considered an "invalid operation". When $\lambda > 1$, the bending bracket trajectory forms a buckle ring pattern. From the longest horizontal cross string of the buckle ring, the points on the trajectory exhibit horizontal velocities opposing the direction of travel of the machine. Accordingly, the bending bracket imparts a backward propulsion of horizontal velocity to the trellis pole. Thus, the operational requirements of the bending bracket are satisfied; this is classified as an "effective operation". Therefore, the necessary condition for the normal operation of the bending stent necessitates that its speed ratio $\lambda > 1$.

As evident from Figure 4, for $\lambda > 1$, the bending bracket end moves from point $A_0$ to $A_1$ by time $t_1$. The combined motion of the machine travel and bending bracket circular motion ensures that the horizontal partial velocity at point $A_1$ is 0. At this instant, the bending bracket end exhibits only vertical downward velocity, and $A_1A_3$ marks the longest

transverse chord. The bending component achieves zero speed, minimizing soil impact on the pole; this improves the planting quality. Therefore, the bending component is required to insert the pole into the soil at point $A_1$. This is mathematically expressed as follows:

$$v_x = v_m - R\omega \sin \omega t_1 = 0, \tag{4}$$

$$\sin \omega t_1 = \frac{v_m}{R\omega} = \frac{1}{\lambda}, \tag{5}$$

$$\cos \omega t_1 = \sqrt{1 - \sin^2 \omega t_1} = \frac{\sqrt{\lambda^2 - 1}}{\lambda}. \tag{6}$$

On the basis of Equations (3)–(5), $t_1$ can be obtained as

$$t_1 = \frac{\arcsin(1/\lambda)}{\omega} \tag{7}$$

The bending bracket $A_1$ moves to the lowest point $A_2$ of the residual pendulum line (i.e., the lowest point of the circular motion of the bending bracket) after time $t_2$, which can be obtained as

$$t_2 = \frac{\pi}{2\omega} \tag{8}$$

Substituting $t_1$ and $t_2$ into Equation (1), the coordinates of the position of points $A_1$ and $A_2$ of the bending bracket $(x_1, y_1)$ and $(x_2, y_2)$, respectively, can be determined as follows:

$$\begin{cases} x_1 = v_m \frac{\arcsin(1/\lambda)}{\omega} + \frac{R \cdot \sqrt{\lambda^2 - 1}}{\lambda} = \frac{R}{\lambda}\left(\arcsin\frac{1}{\lambda} + \sqrt{\lambda^2 - 1}\right) \\ \mathrm{y}_1 = H - \frac{R}{\lambda} \end{cases}, \tag{9}$$

$$\begin{cases} x_2 = v_m \frac{\pi}{2\omega} = \frac{\pi R}{2\lambda} \\ y_2 = H - R \end{cases}. \tag{10}$$

The range of action $b$ of the bending bracket on the trellis pole is half the distance of the longest transverse chord $A_1A_3$ of the cosine "loop buckle".

$$b = x_1 - x_2 = \frac{R}{\lambda}\left(\arcsin\frac{1}{\lambda} + \sqrt{\lambda^2 - 1} - \frac{\pi}{2}\right) \tag{11}$$

The vertical height $c$ at the end of the bending bracket acting on the shed pole (i.e., the vertical distance below the longest horizontal chord of the remaining pendulum loop buckle) is given by

$$c = y_1 - y_2 = R(1 - \frac{1}{\lambda}). \tag{12}$$

Upon setting the number of planting arm groups $Z$ as 2, the distance between the two groups of neighboring planting arms in the movement of the residual pendulum line produced by the ring buckle is defined as pitch $L$, that is, the length of A1B1.

$$L = v_m \frac{2\pi}{Z\omega} = \frac{2\pi R}{Z\lambda} \tag{13}$$

Figure 5 shows the trajectory of the pressing rod arm. During the bending insertion frame operation, the pressing rod arm is squeezed by the bending plate, rotating around the pressing rod arm shaft, from point a to the lower end of the movement to point b. Thus, planting is completed. The pressing rod arm is then disengaged, moving along the trajectory to return to point a and completing the cycle.

The horizontal direction away from the center of rotation of the pressure pressing rod arm is considered the positive $X$-axis direction. The upward direction, perpendicular to the

*X*-axis, over the center of rotation is considered the positive *Y*-axis direction. The trajectory equation of any point on the pressing rod arm can be expressed as

$$\begin{cases} x = r\cos\omega t \\ y = r\sin\omega t \end{cases}. \tag{14}$$

where $t$ is the pressing rod arm rotation time (s); $r$ is the length of the pressing rod arm (mm); and $\omega$ is the pressing rod arm rotational angular velocity (rad/s).

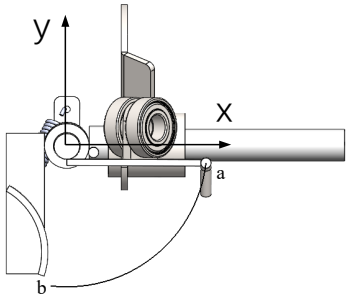


**Figure 5.** Pressing rod arm motion trajectory. Note: a represents the starting position of the pressing rod arm and b represents the rotating movement of the pressing rod arm to the lower position.

### *2.3. Rotary Double-Insertion Device Construction Parameters*

The side of the trellis pole, after bending into the ground, is shown in Figure 6. When the center of the rotary axis is a certain height above the ground, the length of the bending bracket and length of the pressing rod arm affect the distance from the ground. The agronomic requirements stipulate the construction of small arched greenhouses by using poles that are 0.6 cm in diameter and 160 cm in length, yielding a good arch span of 73 cm. To ensure that the bending pressure plate at the lowest point does not contact the soil to interfere with the normal movement, a certain distance must be allowed.

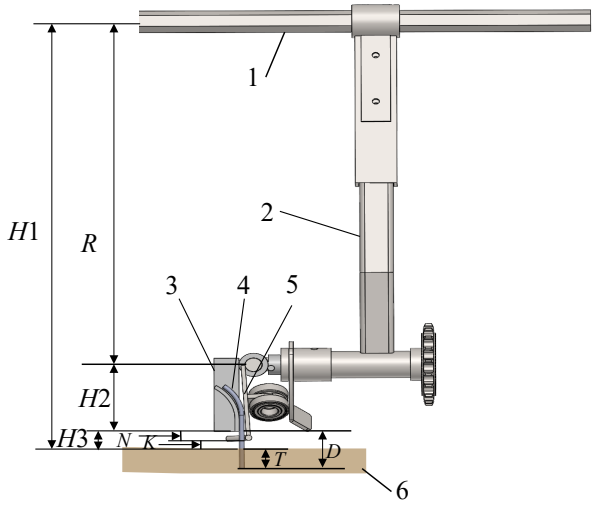


**Figure 6.** Diagram of the shed pole inserted into the soil. (1) Rotary shaft; (2) bending bracket; (3) bending bearing plate; (4) part of the shed pole; (5) pressing rod arm; and (6) soil. Note: $H1$ represents the distance from the center of the rotary shaft to the ground (mm); $R$ denotes the length of the bending bracket (mm); $H2$ represents the length of the bending bearing plate (mm); $H3$ is the distance between the lower end of the bending bearing plate and the ground when the planting arm moves to the lowest point (mm); $N$ represents the length of the pressing rod arm over the lower end of the bending bearing plate (mm); $K$ denotes the distance of the pressing rod arm from the ground (mm); $T$ is the depth of insertion for the shed pole into the soil (mm); and $D$ represents the distance between the end of the bending bearing plate and the end of the shed pole into the soil (mm).

On the basis of Figure 6, the depth of the trellis after insertion into the soil can be calculated as

$$H1 + T = R + H2 + D. \tag{15}$$

The planting arm of the insertion frame mechanism rotates, and the height from the ground when it moves to the lowest point is given as

$$D = K + T. \tag{16}$$

To ensure that the pressure rod arm and the shed pole bending have sufficient contact in real scenarios, the pressure rod arm $H2$ has a preliminary selection of 10 cm. To increase the stability of the inserted frame, the height of the center of the rotary shaft should be reduced. Further, the pressure rod arm should be set at a distance of 3 cm off the ground, according to Equations (15) and (16). Based on the agronomic parameters of small arched greenhouses and wheel diameters, the length of the bending bracket is set to 67 cm.

### *2.4. Motion Simulation of Rotary Double-Insertion Device*

To study the movement characteristics and trajectory changes of the planting arm, a kinematics simulation of the planting arm is performed by considering different planting speed ratios. Changes in the static and the dynamic trajectories are examined, and the linkage law between the planting arm speed ratio and the trajectory is analyzed, seeking the suitable planting arm trajectory. In the simulation, the end of the bending plate is selected as the trajectory movement point.

The velocity of the end of the bending plate continuously varies throughout each rotational cycle, with its static trajectory tracing the minimum radius of the inner circle (Figure 7). We perform a comparative analysis focusing on the ratio of its velocity and the machine travel velocity.

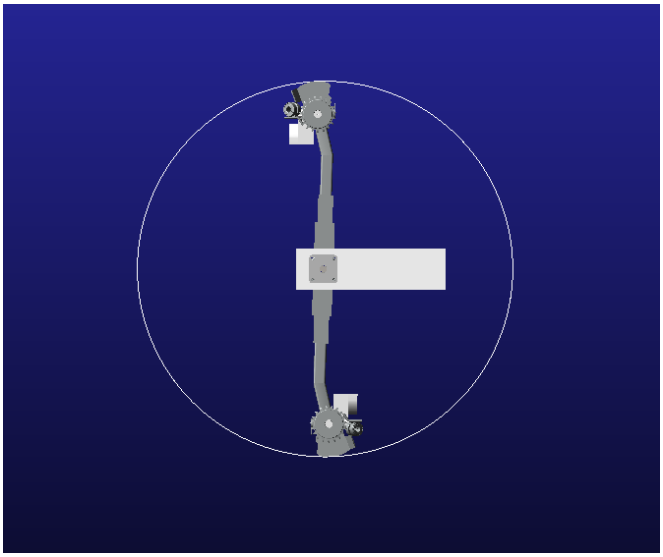

**Figure 7.** Static motion trajectory of the end of the bending plate.

In the design of the planting arm in this study, the central rotary axis is positioned as the geometric center of rotation for the bending bracket end trajectory, with the smallest internal circle radius of 625 mm. The bending bracket end speed is set at 20 r/min. When ratio $\lambda$ equals 1, the corresponding machine travel speed is found to be 0.31 m/s. The dynamic motion trajectory of the bending bracket end with respect to the machine travel speed is shown in Figure 8.

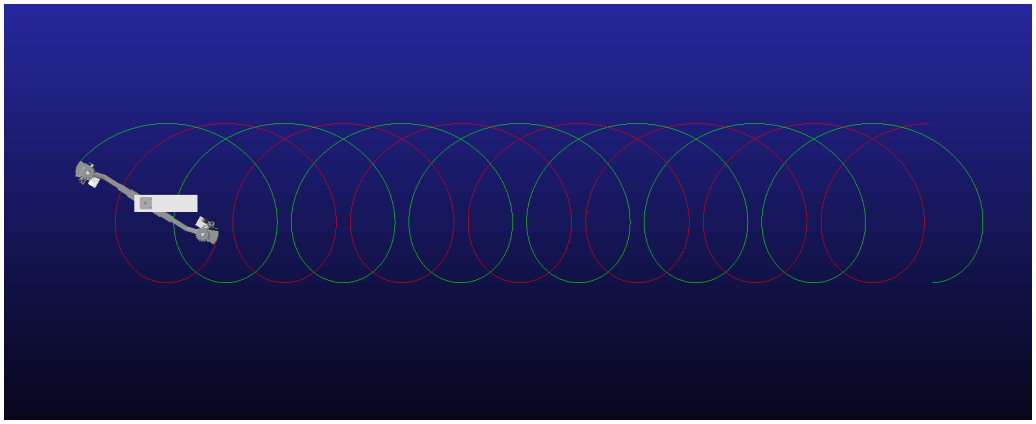

**Figure 8.** Dynamic trajectory of the end of the bending plate ($\lambda$ = 1).

As shown in Figure 8, for a machine travel speed of 0.31 m/s, a snap ring forms in the dynamic motion trajectory of the end of the bending bracket, indicating that the corresponding planting arm rotary radius exactly equals the minimum inner circle radius (i.e., 625 mm) of the static trajectory of the end of the bending bracket centered on the central rotary axis. However, the interval between the snap rings is considerably large, potentially leading to poor land utilization. This indicates that the planting speed ratio at $\lambda < 1$ is appropriate.

To examine the planting speed ratio at $\lambda < 1$, we set the bending bracket rotational speed to 20 r/min and the machine traveling speed to 0.28 m/s. The bending bracket end trajectory then shows a grommet cross (Figure 9), affecting the actual operation.

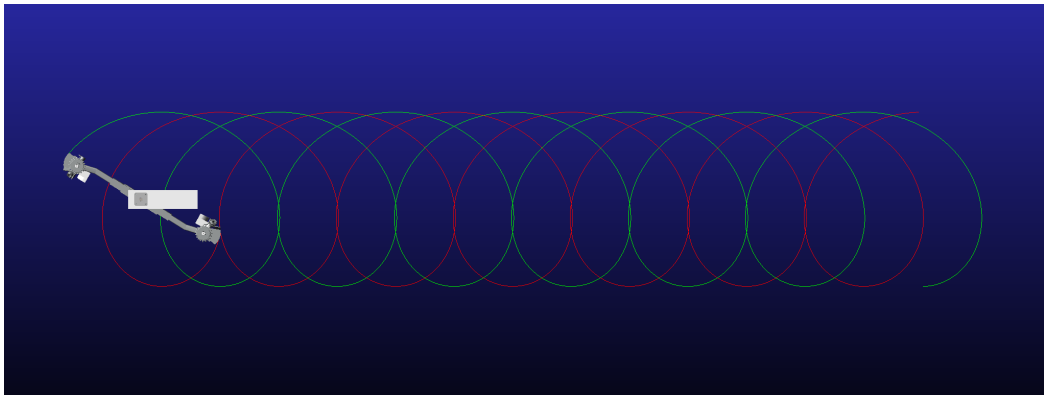

**Figure 9.** Dynamic trajectory of the end of the bending plate ($\lambda$ = 0.69).

Maintaining the bending bracket rotational speed, the machine traveling speed is set to 0.29 m/s. Then, $\lambda$ = 0.71, and the motion trajectory is as depicted in Figure 10. The motion trajectory of the bending bracket is close to the front and back and does not cross the influence, and is periodically arranged. The entire motion process is efficiently distributed. Thus, for $\lambda < 1$, a reasonable adjustment of the machine traveling speed and planting arm slewing speed is conducive to improving the efficiency of planting and the operation effect.

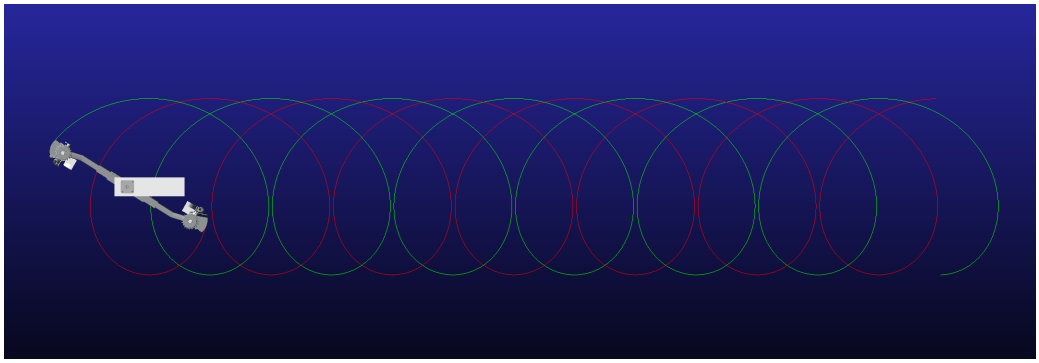

**Figure 10.** Dynamic trajectory of the end of the bending plate ($\lambda$ = 0.71).

### *2.5. Test Material*

The test was conducted at the Nanjing Agricultural Mechanization Research Institute of the Ministry of Agriculture and Rural Affairs, Nanjing, China. The test materials comprised trellis poles (6 mm diameter and 1600 mm length). Measuring instruments included a 5 m tape measure, 300 mm steel ruler, and soil hardness tester (TYD-2, manufactured by Zhejiang topu yunnong Technology Co., Ltd., headquartered in Hangzhou, China. Maximum pressure: 1 kN, measuring depth: 0–400 mm, precision: ±0.5%, resolution: 0.1 kg). Before the test, a trial production of a rotary double-insertion device frame was processed, a real situation of the insertion frame was simulated, using a 653 mm × 435 mm × 305 mm pressure-resistant plastic box filled with soil (the soil was classified as sandy, with an 80% sand and 20% clay composition, and the average values of soil bulk density and moisture content were 1.50 g/cm$^3$ and 2.8%, respectively), and soil compactibility was measured by using a soil hardness tester to achieve the data with the research in line with the test carried out only after the test, the test frame, and the site, as shown in Figure 11.

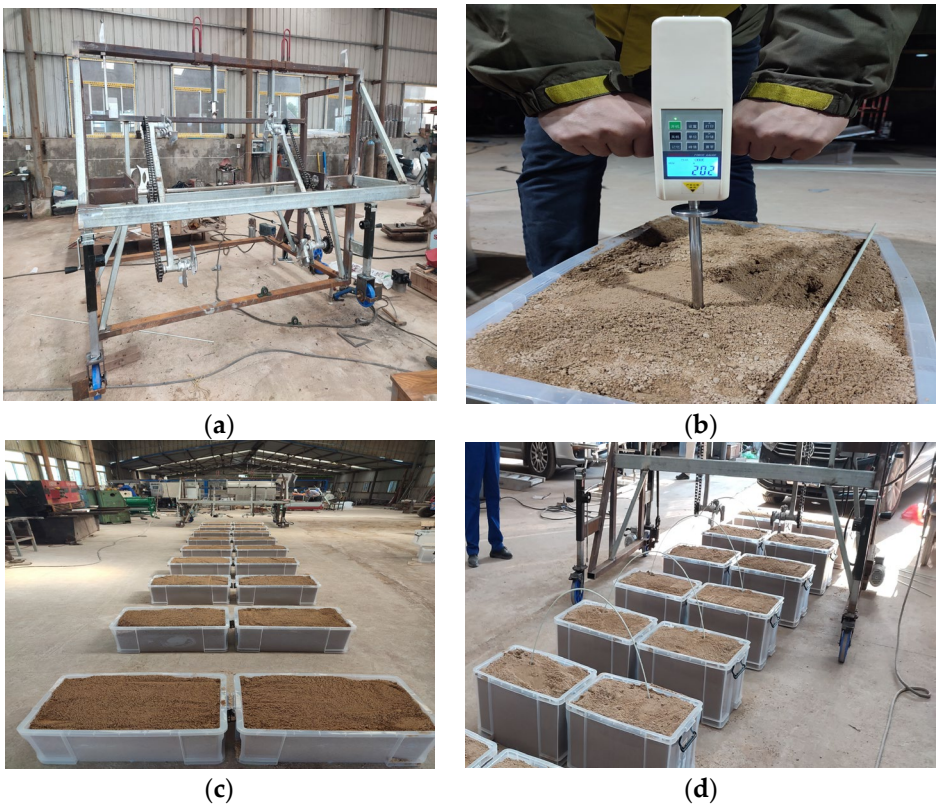

**Figure 11.** Bench test of rotary double-insertion device. (**a**) Bench processing; (**b**) measurement of soil compactness; (**c**) before insertion test; and (**d**) after insertion test.

### *2.6. Evaluation Indicators and Measurement Methods for Rotary Double-Insertion Device*

The scaffolding pass rate was used as an evaluation index for the rotary double-insertion device. However, assessing the pass rate alone was challenging as the width-to-height ratio was fixed after the bending of the scaffolding. Therefore, parameter *K*—-the ratio of the height and span of the small arched scaffolding after the bending and insertion of the scaffolding—-was employed.

$$K = \frac{H}{L} \tag{17}$$

The agronomic parameters of the small arched trellis considered in this study were based on the standard *K*-value of 0.53. The qualification rate of each trellis was determined by comparing its *K*-value with the standard *K*-value. Each group of experiments was repeated three times, and the average values were used for the analyses.

## 3. Results and Discussion

### *3.1. Box–Behnken Center Combination Test and Analysis*

The preliminary tests of the rotary double-insertion device revealed that the qualification rate of the trellis was affected by (A) the planting speed ratio, (B) the center distance of the planting arm group, and (C) the length of the compression pole arm. To investigate the influence of these factors on the qualification rate, a three-factor and three-level Box–Behnken response surface method was used. The experimental design was carried out using Design-Expert 13 software (Version:13.0.1.0 64-bit, manufactured by Stat-Ease, headquartered in Minneapolis, MN, USA) [31]. Further, 17 groups of tests were conducted. The coded levels of the test factors are presented in Table 1. The range of planting speed ratio was obtained through ADAMS (Version: Adams 2020, manufactured by MSC Software Corporation, Newport Beach, CA, USA) simulation, which analyzed the motion trajectory of the rotary double- insertions. The planting speed ratio of 0.7 was found to achieve a high qualification rate for the trellis. Therefore, the range of planting speed ratio was set to 0.6–0.8. The dimensions of the trellis were 730 mm wide and 160 mm high. Following a series of preliminary tests on the bending properties of trellis poles, it was determined that the better center distance for the planting arm was 550 mm. Given the dimensions of the machine, the center distance of the planting arm was set at 500–600 mm, and the length of the pressing rod arm was determined according to the width of the trellis and the distance that the rotary double- insertion device would not interfere with the soil when it was rotated to the lowest point. The requisite width of the trellis was 730 mm, and the length of the pressing arm rod was 95 mm when the bending effect was more in line with the requirements, and the rotary double- insertion device turned to the lowest point without interfering with the soil. Therefore, the length of the pressing rod arm was determined as 80–110 mm.

**Table 1.** Coding table of test factor levels.

| Code Value | Planting Speed Ratio [A] | Planting Arm Center Distance [B] (mm) | Length of Pressing Rod Arm [C] (mm) |
|---|---|---|---|
| −1 | 0.6 | 500 | 80 |
| 0 | 0.7 | 550 | 95 |
| 1 | 0.8 | 600 | 110 |

During the test, a small arched shed was examined using a bench prototype, and the passing rates of the trellis were recorded. The running speed of the mechanism was controlled by a governor, while the center distance of the planting arm was adjusted by increasing or decreasing the bushing size. Further, variation in the length of the pressing rod arm was achieved by using arms of different lengths. Table 2 presents the test results.

**Table 2.** Test program and results.

| Test No. | Planting Speed Ratio | Planting Arm Center Distance(mm) | Length of Lever Arm (mm) | Scaffold Pass Rate (%) |
|---|---|---|---|---|
| 1 | 0.7 | 550 | 95 | 98 |
| 2 | 0.8 | 550 | 80 | 95 |
| 3 | 0.7 | 600 | 110 | 87 |
| 4 | 0.6 | 500 | 95 | 83 |
| 5 | 0.6 | 600 | 95 | 85 |
| 6 | 0.7 | 550 | 95 | 97 |
| 7 | 0.8 | 550 | 110 | 88 |
| 8 | 0.7 | 600 | 80 | 82 |
| 9 | 0.6 | 550 | 80 | 86 |
| 10 | 0.8 | 500 | 95 | 90 |
| 11 | 0.7 | 500 | 110 | 81 |
| 12 | 0.7 | 550 | 95 | 94 |
| 13 | 0.7 | 550 | 95 | 92 |
| 14 | 0.8 | 600 | 95 | 96 |
| 15 | 0.6 | 550 | 110 | 87 |
| 16 | 0.7 | 550 | 95 | 91 |
| 17 | 0.7 | 500 | 80 | 85 |

This study applied Design-Expert 13 software to perform the regression analysis on the experimental results that are shown in Table 2. The non-significant terms were excluded to obtain the ternary quadratic regression equation of the trellis qualification rate and the parameters $A$, $B$, and $C$, as shown in Equation (18). The scaffold pass rate model $p < 0.01$ indicated that the generated regression model was highly significant, and its coefficient of determination $R^2 = 0.9475$, with fixed coefficient close to 1, indicated that the regression model can describe most of the quantitative relationships of the experimental data. The test of loss of fit, $p > 0.05$, indicated no loss of fit, suggesting that the regression equation was well-fitted, and the results are shown in Table 3.

$$K = 98 + 3.13A + 1.38B - 0.75C + 2AB - 1.75AC + 2.25BC - 1.25A^2 - 6.25B^2 - 8C^2. \quad (18)$$

**Table 3.** Analysis of variance for scaffold pass rates.

| Source of Error | Sum of Squares | df | Mean Square Sum | F-Value | *p*-Value | Significance |
|---|---|---|---|---|---|---|
| Model | 621.28 | 9 | 69.03 | 39.45 | <0.0001 | ** |
| $A$ | 78.13 | 1 | 78.13 | 44.64 | 0.0003 | ** |
| $B$ | 15.13 | 1 | 15.13 | 8.64 | 0.0217 | * |
| $C$ | 4.50 | 1 | 4.50 | 2.57 | 0.1528 | |
| $AB$ | 16.00 | 1 | 16.00 | 9.14 | 0.0193 | * |
| $AC$ | 12.25 | 1 | 12.25 | 7.00 | 0.0331 | * |
| $BC$ | 20.25 | 1 | 20.25 | 11.57 | 0.0114 | * |
| $A^2$ | 6.58 | 1 | 6.58 | 3.76 | 0.0937 | * |
| $B^2$ | 164.47 | 1 | 164.47 | 93.98 | <0.0001 | ** |
| $C^2$ | 269.47 | 1 | 269.47 | 153.98 | <0.0001 | ** |
| Residuals | 12.25 | 7 | 1.75 | | | |
| Misfit term | 12.25 | 3 | 4.08 | 1.77 | 0.3810 | |
| Error | 10.8 | 4 | 2.7 | | | |
| $R^2$ | 0.9475 | | | | | |

** Means highly significant, * means significant.

Response surface curves were generated using Design-Expert 13 (Figure 12). One of the test factors—$A$, $B$, or $C$—was located at the 0 level, and the effects of the interaction of the other two factors were analyzed based on the response surfaces.

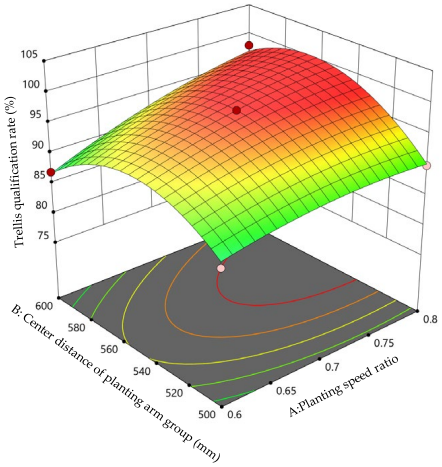


**Figure 12.** Response surface diagram of the interaction between the center distance of the planting arm and the planting speed ratio.

The response surface curves of the interaction between the planting arm center distance and the planting speed ratio on the trellis qualified rate when the length of the pressing rod arm was located at the center level (95 mm) are shown in Figure 12. When the planting speed ratio was fixed at a certain level, the trellis qualified rate increased and then decreased with the increase in the center distance of the planting arm group, and the optimal range of the center distance of the planting arm group was 540–560 mm. When the center distance of the planting arm group was fixed at a certain level, the trellis qualified rate increased with the increase in the planting speed ratio and then tended to be flat. Therefore, the optimal range of the planting speed ratio was 0.7–0.75.

When the center distance of the planting arm group was located at the center level (550), the response surface plot of the interaction between the planting speed ratio and the length of the pressing rod arm on the trellis qualified rate is shown in Figure 13. When the planting speed ratio was fixed at a certain level, the trellis qualification rate increased sharply with the increasing length of the pressing rod arm, with the optimal range of the length of the pressing rod arm being 86–98 mm. When the length of the pressing rod arm was fixed at a certain level, the trellis qualification rate increased sharply with the increasing planting speed ratio, with the optimal range of the planting speed ratio being 0.65–0.75.

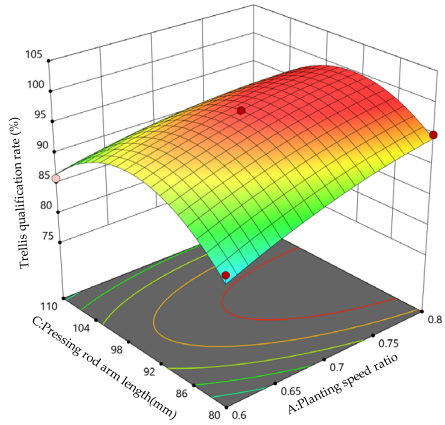


**Figure 13.** Response surface diagram of the interaction between planting speed ratio and pressing rod arm length.

When the planting speed ratio was located at the center level (0°), the response surface plot of the interaction between the center distance of the planting arm group and the length of the pressing rod arm on the trellis pass rate is shown in Figure 14. When the

center distance of the planting arm group was fixed at a certain level, the trellis qualified rate increased gradually with the increasing length of the pressing rod arm, with the optimal range of the length of the pressing rod arm being 92–104 mm. When the length of the pressing rod arm was fixed at a certain level, the trellis qualified rate increased and decreased sharply the with increasing center distance of the planting arm group, with the optimal range of the planting arm center distance being 540–560 mm and the optimal range being 540–560 mm. Thus, the optimal range was 540–560 mm.

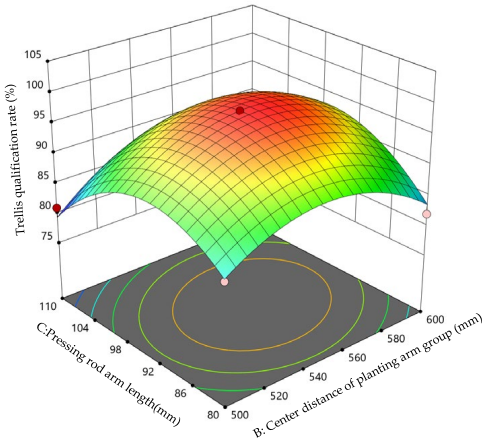


**Figure 14.** Response surface diagram of the interaction between the center distance of the planting arm group and the length of the pressing rod arm.

### *3.2. Parameter Optimization*

For obtaining the best combination of operating parameters for the planting arm and improvement of the trellis qualification rate, the experimental results of the indoor bench work were optimized using the optimization module of Design-Expert 13. To achieve the highest trellis qualification rate, the constraints of Equation (19) were established.

$$\begin{cases} \min k(A,B,C) \\ \begin{cases} 0.65 < A < 0.75 \\ 540 \text{ mm} < B < 560 \text{ mm} \\ 86 \text{ mm} < C < 104 \text{ mm} \end{cases} \end{cases} \tag{19}$$

Software analysis revealed the optimal combination of the working parameters of the planting arm as follows: planting speed ratio of 0.702; center distance of the planting arm group of 554.068 mm; and length of pressing rod arm of 92.895 mm, resulting in a trellis qualification rate of 98.05%.

Utilizing the optimal parameter combination, the bench device was accordingly adjusted, and indoor operation tests were re-conducted. The model results were then verified. On the basis of the actual working condition requirements of the planting machinery and rounded optimized theoretical values, the test conditions were set at a planting arm planting speed ratio of 0.7, planting arm center distance of 554 mm, and length of pressing rod arm of 93 mm. The test results were sampled thrice to obtain average values, and the effect of random error was removed. The average value of the measured trellis qualification rate was 96.73%, and the relative error between the test value and optimized value was 1.32%, which was highly consistent with the results. Thus, the reliability of the optimal parameter combination was verified.

### *3.3. Field Tests*

This experiment was conducted in the cantaloupe test area of Hami City, Xinjiang, and the average value was taken after three trials with the best combination of parameters. The operating distance of the hanging small arched insertion machine was 20 m, and the

test was repeated thrice. The soil type of the test site was sandy soil. For a soil moisture content of 2.5% and depth of 200 mm, the soil compactness was 165 N/cm$^2$; this was consistent with the results in the literature. In the test, the arbor insertion machine was in good operating condition, and the insertion situation was stable. Tools such as a tape measure, stopwatch, and steel ruler were used to acquire the measurements. Prior to the test, the tractor forward speed was set to 1.2 km/h, and the navigation was appropriately configured. The field test site is shown in Figure 15.

**Figure 15.** Rotary double-insert rack-mounted job scaffolding diagrams.

In the field test, the rotary double-insertion device in the planting speed ratio was 0.72, the trellis qualified rate was 95.32%, in line with the small arch shed insertion device design requirements. The measurement process found that the overall operating conditions of the trellis pole, jumping pole, leakage pole, etc., were good.

### *3.4. Discussion*

This study observed that the response surfaces of the trellis qualified rate in Figures 12–14 showed a convex shape, and optimum values existed for the planting speed ratio, planting arm group center distance, and length of pressing rod arm. The reason for this situation is that, in order to ensure that the planting arm has a better bending effect on the shed pole and to avoid the trellis spacing being too large, the planting speed ratio should be selected in the appropriate variation interval. When the value is too large, the planting arm rotary speed is too fast, which increases the shed pole due to the violent collision with the planting arm caused by the shedding of the situation. When the value is too small, the residual oscillation line of the rotary double- insertion device trajectory becomes broader and larger, which leads to a long operating time, the trellis spacing is too large, the trellis is not easy to insert into the soil, and the trellis qualified rate is reduced. The center distance of the planting arm group also needs to be selected within the appropriate change interval. When the center distance between the two planting arms is too tiny, the shed pole cannot easily be bent out of the target arch. With the increased center distance of the planting arm group, the trellis qualification rate gradually increases. When the center distance is too large, the shape of the trellis is wider and smaller in height, which is not in line with the requirements of the target trellis, resulting in a low trellis qualified rate. The primary role of the pressure rod arm is to bend the shed pole and the length also needs to be selected in the appropriate range. When the length of the pressure rod arm is too small, it is difficult to clamp the shed pole and keep the state in the bending process, which easily leads to the shed pole falling off. With the gradual increase in the length of the pressing rod arm, the trellis qualification rate gradually increases. When the length of the pressing rod arm is too big, the slewing process easily intervenes with the machine and the soil, which leads to a lower trellis qualification rate.

In the process of building small arched trellises, the appropriate width-to-height ratio of the trellis is crucial to the growth of the crop. The larger the height, the more favorable it is for the crop to obtain sufficient light and growth space under the condition of satisfying the width. After the trellis is bent, the width-to-height ratio becomes a fixed value. Therefore,

to improve the trellis qualification rate, a rotary double-insertion device was designed in this study, and a mathematical regression model of the qualification rate of the trellis with the planting arm was established. A qualification rate of 98.05% and qualification rate of 95.74% were achieved in the field test. The relative error between the actual test value and optimized value of the regression equation in the field was 2.31%, which was consistent with the well-established results on the trellis qualification rate. The three-way quadratic equation with planting speed ratio, center distance of planting arm group, and length of pressing rod arm was accurate and reliable, thus meeting the agronomic requirements of small arched greenhouse construction.

Small arched greenhouse construction machinery is increasingly used in downtime bending planting or planting requiring bending molded metal arches and other forms. In actual operation, there may be a low operating speed or explosive shed pole material that, for instance, is difficult to store and transport, thereby seriously affecting the quality of the operation.

Owing to the complexity of the field operating environment, there may be hard stones or other debris, and excessive bumps may case trellis poles to fall off. In addition to the impact of the tractor crushing, the soil tightness also varies. If the soil tightness is excessively high, the trellis cannot be planted into the soil, leading to a low trellis qualification. Therefore, when addressing different soil types and environments, the rotary double-plugging device must be studied in terms of its stability. The two rows of furrowing knives set in front of the rotary double- insertion device can effectively remove the interference of stones or debris in front of the planting position. Simultaneously, they can loosen the soil to ensure that the trellis is planted deep into the soil. In different soil types, there may be larger or harder stones and other hard objects, which may easily cause deformation or breakage of the furrowing knives; thus, it is necessary to level the field before operation and optimize the structure of the furrowing knives or select the furrowing knives made of better materials. The shortcomings noted herein will be further studied and solved in future experiments.

## 4. Conclusions

(1) By analyzing the process of small arched trellis skeleton construction, according to the kinematics principle that the traveling motion of the machine and the rotation of the parts themselves are combined into a composite motion, a rotary double-insertion device was designed, and a test stand was built to conduct a three-factor three-level Box–Behnken response surface test on the trellis qualification rate. The test results showed that the trellis qualified rate was mainly affected by the planting speed ratio, center distance of the planting arm group, and length of the pressing rod arm. The optimal ranges of the planting speed ratio, center distance of the planting arm group, and length of the pressing rod arm were 0.65–0.75, 540–560 mm, and 86–104 mm, respectively.

(2) Design-Expert 13 software was used to analyze the results and basis of the actual working condition requirements of the planting machinery and optimized theoretical values were rounded to obtain the optimal parameter combination as follows: planting speed ratio, 0.7; planting and inserting arm group center distance, 554 mm; length of pressing rod arm, 93 mm; and trellis qualified rate, 98.05%. Based on the optimal parameter combination, the insertion mechanism was optimized and tested again, with the average value of the measured trellis qualification rate being 96.73%, and the relative error between the test value and theoretical optimization value being 1.32%. The model accuracy was high, thus verifying the reliability of the optimal parameter combination.

(3) Field insertion test results showed that, with the rotary double-insertion device at the planting speed ratio of 0.7, the trellis qualified rate was 95.74% compared with the theoretical optimization value of 2.31% error in line with the design requirements of a small arched greenhouse insertion device. There was no trellis pole jumping

pole, leakage pole, or damage. Moreover, if the overall operating conditions are favorable, a small arched greenhouse insertion device design and optimization can serve as a suitable reference. The overall operation was good, and the findings of this study can therefore serve as a basis for the design and optimization of the small arbor insertion device.

**Author Contributions:** Conceptualization, J.H. and Y.G.; methodology, J.H., X.C. and Y.G.; software, J.H. and X.C.; validation, J.H. and X.C.; formal analysis, J.H., Y.G. and X.C.; investigation, J.H.; resources, Y.G., X.C.; data curation, J.H.; writing—original draft preparation, J.H.; writing—review and editing, J.H. and Y.G.; visualization, J.H. and X.C.; supervision, X.C. and Y.G.; project administration, X.C. and Y.G.; funding acquisition, X.C. and Y.G. All authors have read and agreed to the published version of the manuscript.

**Funding:** This research was supported by the Key Research and Development Program of Xinjiang Uygur autonomous region, China (2023B02017) and the China Agriculture Research System (Grant No. CARS-25).

**Institutional Review Board Statement:** Not applicable.

**Data Availability Statement:** The data presented in this study are available in the article.

**Acknowledgments:** We sincerely appreciate the careful and precise reviews by anonymous reviewers and editors. We also acknowledge the contribution of Xiaozhong Deng and Xinguo Pang to the manuscript.

**Conflicts of Interest:** The authors declare that they have no competing interests.

## References

1. Sun, J.; Gao, H.-B.; Tian, J.; Wang, J.-W.; Du, C.-X.; Guo, S.-R. Development status and trends of protected horticulture in China. *J. Nanjing Agric. Univ.* **2019**, *42*, 594–604.
2. Chen, Y.; Li, Z.; Zhang, W.; Zhang, W.; He, J. Research progress and development countermeasures of facility agriculture suitable for mechanization. *J. Agric. Eng.* **2022**, *12*, 22–24.
3. Xiaoming, W.; Fei, Q.; Xiaoming, D.; Shunshu, B.; Zhonghua, L.; Fen, H. Main achievements in China facility horticulture. *J. Agric. Mech. Res.* **2010**, *32*, 227–231.
4. López-Aranda, J.M.; Soria, C.; Santos, B.M.; Miranda, L.; Domínguez, P.; Medina-Mínguez, J.J. Strawberry production in mild climates of the world: A review of current cultivar use. *Int. J. Fruit Sci.* **2011**, *11*, 232–244. [CrossRef]
5. Lopez-Martinez, A.; Molina-Aiz, F.D.; de Los Angeles Moreno-Teruel, M.; Pena-Fernandez, A.; Baptista, F.J.F.; Valera-Martinez, D.L. Low tunnels inside mediterranean greenhouses: Effects on air/Soil temperature and humidity. *Agronomy* **2021**, *11*, 1973. [CrossRef]
6. Hernandez, J.; Soriano, T.; Morales, M.I.; Castilla, N. Row covers for quality improvement of Chinese cabbage New Zealand. *J. Crop Hortic. Sci.* **2004**, *32*, 379–388. [CrossRef]
7. Gimenez, C.; Otto, R.; Castilla, N. Productivity of leaf and root vegetable crops under direct cover. *Sci. Hortic.* **2002**, *94*, 1–11. [CrossRef]
8. Moreno, D.A.; Víllora, G.; Ruiz, J.M.; Romero, L. Growth conditions, elemental accumulation and induced physiological changes in Chinese cabbage. *Chemosphere* **2003**, *52*, 1031–1040. [CrossRef]
9. Chen, Z.L.Z.; Yan, T.; Huang, Y.; Huang, J.; Huang, Z. The effects of arch plastic mulching on the chief agronomic traits and revenue of chewing cane. *Sugarcane Canesugar* **2022**, *51*, 22–26.
10. Li Qiuling, L.G.; Chuncheng, Z. Preliminary study on cutting and seedling raising technology of small arch shed of wild large leaf tea tree in Liu Xiang, Jinxiu. *J. Guangxi Agric.* **2020**, *35*, 38–40.
11. Sideman, R.G.; Brown, A.; Martin, C.A.; Hazzard, R.; Cavanagh, A. Temperature moderating effects of low tunnels over winter in cool climates. *Hortscience* **2012**, *47*, S404–S405.
12. Castilla, P.N. *Invernaderos de Plástico. Tecnología y Manejo*; Ediciones Mundi-Prensa: Madrid, Spain, 2007.
13. Willden, S.A.; Pritts, M.P.; Loeb, G.M. The effect of plastic low tunnels on natural enemies and pollinators in New York strawberry. *Crop Prot.* **2022**, *151*, 105820. [CrossRef]
14. Orde, K.M.; Marini, R.; Demchak, K.; Sideman, R. Albion strawberry responds to mulch treatments and low tunnels covered with photoselective films. *Hortscience* **2021**, *56*, 1005–1014. [CrossRef]
15. Duhan, A.; Singh, D.; Kumar, A.; Maan, D.S. Effect of low plastic tunnels, transplanting dates and mulching on quality of tomato Indian. *J. Agric. Sci.* **2021**, *91*, 1675–1678. [CrossRef]
16. Jenni, S.; Dubuc, J.F.; Stewart, K.A. Plastic mulches and row covers for early and midseason crisphead lettuce produced on organic soils. *Can. J. Plant Sci.* **2003**, *83*, 921–929. [CrossRef]

17. Orde, K.M.; Sideman, R.G. Low tunnel and cultivar effects on day-neutral strawberry yield and characteristics in New Hampshire. *Horttechnology* **2019**, *29*, 795–810. [CrossRef]
18. Lewers, K.S.; Fleisher, D.H.; Daughtry, C.S.T. Low Tunnels as a strawberry sreeding tool and season-extending production System. *Int. J. Fruit Sci.* **2017**, *17*, 233–258. [CrossRef]
19. Nordey, T.; Ochieng, J.; Ernest, Z.; Mlowe, N.; Mosha, I.; Fernandes, P. Is vegetable cultivation under low tunnels a profitable alternative to pesticide use? The case of cabbage cultivation in northern Tanzania. *Crop Prot.* **2020**, 134. [CrossRef]
20. Bekraoui, A.; Chakir, S.; Fatnassi, H.; Mouqallid, M.; Majdoubi, H. Climate behaviour and plant heat activity of a citrus tunnel greenhouse: A computational fluid dynamic study. *Agri Eng.* **2022**, *4*, 1095–1115. [CrossRef]
21. Henschel, J.M.; Resende, J.T.V.; Giloni-Lima, P.C.; Zeist, A.R.; Lima Filho, R.B.; Santos, M.H. Production and quality of strawberry cultivated under different colors of low tunnel cover. *Hortic. Bras.* **2017**, *35*, 364–370. [CrossRef]
22. Arancibia, R.A.; Motsenbocker, C.E. Differential watermelon fruit size distribution in response to plastic mulch and spunbonded polyester rowcover. *Horttechnology* **2008**, *18*, 45–52. [CrossRef]
23. Faivor, R.M.S. *Low Tunnel Strategies for Microclimate Modification and Early Vegetable Production*; Michigan State University: East Lansing, MI, USA, 2014.
24. Vujasinović, V. *Yield and Quality of Early Potato Depending TI on Agricultural Practices and Argoecological Condicions*; University of Novi Sad: Novi Sad, Serbia, 2016.
25. Liu Ping, W.C.; Hongzheng, Q.; Jialin, H. Design and test of automatic cuttage device for arched shed. *Trans. Chin. Soc. Agric. Eng.* **2020**, *36*, 21–29.
26. Jiang, W.; Deng, J.; Yu, H. Development situation, problems and suggestions on industrial development of protected Horticulture. *Sci. Agric. Sin.* **2015**, *48*, 3515–3523.
27. Chen, K.; Liu, X.; Jin, S.; Li, L.; He, X.; Wang, T.; Mi, G.; Shi, Y.; Li, W. Design of and experiments with an automatic cuttage device for an arch shed pillar with force feedback. *Agriculture* **2022**, *12*, 875. [CrossRef]
28. Wang, Z.W.C.; Zhang, F.; Li, Z.; Wang, D. Research status and development trend of tilm-mulching machinery. *Agric. Equip. Veh. Eng.* **2022**, *60*, 49–54.
29. Lu, K.Z.G.; Peng, S.; Lei, Z.; Fu, J.; Zha, X.; Zhou, Y. Design and performance of tracked harvester for ratoon rice with double-headers and double-threshing cylinders. *J. Huazhong Agric. Univ.* **2017**, *36*, 108–114.
30. Yongwei, S.; Shuhuan, Y.; Shuming, Y. Computer simulation on reel trajectory. *J. Agric. Mech. Res.* **2010**, *32*, 141–145.
31. Shen, G.W.G.; Hu, L.; Yuan, J.; Wang, Y.; Wu, T.; Chen, X. Development of harvesting mechanism for stem tips of sweet potatoes. *Trans. Chin. Soc. Agric. Eng.* **2019**, *35*, 46–55.